Mechanism of force generation by myosin heads in skeletal muscle

18. Zhu, Q. Y., Scarborough, A., Polsky, B. & Chou, T. C. Drug combinations and effect parameters of zidovudine, stavudine, and nevirapine in standardized drug-sensitive and resistant HIV type 1 strains. *AIDS Res. Hum. Retrovir.* **12,** 507–517 (1996).
19. Strauss, P. R., Beard, W. A., Patterson, T. A. & Wilson, S. H. Substrate binding by human apurinic/apyrimidinic endonuclease indicates a Briggs-Haldane mechanism. *J. Biol. Chem.* **272,** 1302–7. (1997).
20. McCullough, A. K., Dodson, M. L. & Lloyd, R. S. Initiation of base excision repair: glycosylase mechanisms and structures. *Annu. Rev. Biochem.* **68,** 255–285 (1999).
21. Chen, D. S., Herman, T. & Demple, B. Two distinct human DNA diesterases that hydrolyze 3′-blocking deoxyribose fragments from oxidized DNA. *Nucleic Acids Res.* **19,** 5907–5914 (1991).
22. Bhagwat, A. S., Sanderson, R. J. & Lindahl, T. Delayed DNA joining at 3′ mismatches by human DNA ligases. *Nucleic Acids Res.* **27,** 4028–4033 (1999).
23. Hoss, M. *et al.* A human DNA editing enzyme homologous to the *Escherichia coli* DnaQ/MutD protein. *EMBO J.* **18,** 3868–3875 (1999).
24. Mazur, D. J. & Perrino, F. W. Identification and expression of the TREX1 and TREX2 cDNA sequences encoding mammalian 3′–5′ exonucleases. *J. Biol. Chem.* **274,** 19655–19660 (1999).
25. Mazur, D. J. & Perrino, F. W. Excision of 3′ termini by the Trex1 and TREX2 3′-5′ exonucleases: characterization of the recombinant proteins. *J. Biol. Chem.* **276,** 17022–17029 (2001).

Supplementary Information accompanies the paper on *Nature*'s website (http://www.nature.com).

Acknowledgements

We thank Z. Hatahet and J. B. Sweasy for discussion; M. Kelley and B. Demple for providing the APE clones; A. Tomkinson for human DNA ligase I; and J. Sweasy for human DNA polymerase β.

Competing interests statement

The authors declare that they have no competing financial interests.

Correspondence and requests for materials should be addressed to Y.C.-C. (e-mail: Cheng.lab@Yale.edu).

Mechanism of force generation by myosin heads in skeletal muscle

Gabriella Piazzesi*, Massimo Reconditi*, Marco Linari*, Leonardo Lucii*, Yin-Biao Sun†, Theyencheri Narayanan‡, Peter Boesecke‡, Vincenzo Lombardi* & Malcolm Irving†

* *Università di Firenze, Viale G.B. Morgagni 63, I-50134 Firenze, Italy*
† *Randall Centre, School of Biomedical Sciences, King's College London, London SE1 1UL, UK*
‡ *European Synchrotron Radiation Facility, F-38043 Grenoble Cedex, France*

Muscles generate force and shortening in a cyclical interaction between the myosin head domains projecting from the myosin filaments and the adjacent actin filaments. Although many features of the dynamic performance of muscle are determined by the rates of attachment and detachment of myosin and actin[1], the primary event in force generation is thought to be a conformational change or 'working stroke' in the actin-bound myosin head[2–8]. According to this hypothesis, the working stroke is much faster than attachment or detachment, but can be observed directly in the rapid force transients that follow step displacement of the filaments[3]. Although many studies of the mechanism of muscle contraction[9–13] have been based on this hypothesis, the alternative view—that the fast force transients are caused by fast components of attachment and detachment[14–17]—has not been excluded definitively. Here we show that measurements of the axial motions of the myosin heads at ångström resolution by a new X-ray interference technique[18] rule out the rapid attachment/detachment hypothesis, and provide compelling support for the working stroke model of force generation.

When the length of an active muscle fibre is decreased suddenly, so that each set of myosin filaments slides by a few nanometres along the neighbouring actin filaments, the force decreases during the length change (Fig. 1a). This reflects the undamped elasticity of the muscle fibre, and is called phase 1 of the force transient[3,19]. After the length change, force recovers at about 1,000 s^{-1} (phase 2). Our aim was to determine whether the phase 2 force recovery is caused by a working stroke in the actin-attached myosin heads[2–8], or by rapid detachment of heads followed by rapid attachment to different actin monomers[14–17].

We measured the axial motion of the myosin heads during the force transients using X-ray interference between the two arrays of myosin heads in each filament (Fig. 1c). Each half of the myosin filament (magenta) contains an array of 49 layers of heads (orange) with a regular spacing d (~14.5 nm). These arrays give rise to an axial X-ray reflection called the M3, with intensity distribution $\sin^2(49\pi Rd)/\sin^2(\pi Rd)$ (Fig. 1d, orange), where R is the reciprocal space parameter. The two arrays are separated by a 'bare zone' of length B (~160 nm), so that their centres are a distance $L = B + 48d$ apart (Fig. 1c). X-ray interference between the two arrays effectively multiplies the intensity distribution by $\cos^2(\pi RL)$ (Fig. 1d, magenta). The resulting fine structure of the X-ray reflection (Fig. 1d, green) provides an extremely sensitive measure of the axial motion of the myosin heads[18].

We recorded the intensity profile of the M3 reflection in a 2-ms period before the length step (Fig. 1a, b, T_0, green), in a 100-μs period close to the end of phase 1 (T_1, red), and in a 2-ms period near the end of phase 2 (T_2, blue). The length step caused a decrease in the relative intensity of the higher angle peak of the M3 reflection, and shifted both peaks to a higher angle (Fig. 1b). These changes are in the direction expected for a decrease of the interference distance (L) between the two arrays of actin-attached myosin heads when the fibre shortens and the actin filaments move towards the centre of the myosin filament (Fig. 1c). Most of the change in L occurred during phase 1 of the force transient (Fig. 1b, green to red).

The changes in interference fine structure of the M3 reflection were expressed as the ratio of the intensity of the higher angle peak

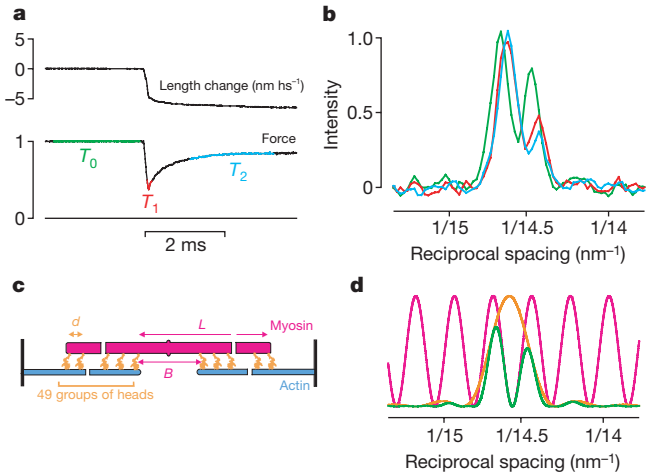

Figure 1 Changes in interference fine structure of the M3 X-ray reflection produced by rapid shortening. **a**, Length change in nanometres per half-sarcomere (hs), and force normalized by isometric force T_0. Fibre cross-sectional area, 27,300 μm^2; T_0, 293 kN m^{-2}; sarcomere length, 2.13 μm. **b**, Axial X-ray intensity distribution of the M3 reflection normalized to that of the lower angle peak. Colours denote the periods T_0, T_1 and T_2 shown in **a**; the total exposure times (equivalent unattenuated beam) were 52, 158, and 105 ms, respectively. **c**, The two arrays of myosin heads (orange) in each myosin filament (magenta). **d**, Axial X-ray intensity distribution (green) calculated as the product of the diffracted intensity from an array of 49 heads with $d = 14.57$ nm (orange) and the interference function for $L = 865.92$ nm (magenta).

to that of the lower angle peak, I_{HA}/I_{LA} (Fig. 2a), and the spacings of the lower and higher angle peaks, S_{LA} and S_{HA} (Fig. 2b). All three parameters decreased as the size of the shortening step was increased, although the changes seemed to saturate for steps larger than 7 nm. The observed changes were similar at T_1 (red circles) and T_2 (blue triangles). The mean spacing of the M3 reflection, S_{M3} (Fig. 2b), which is related to the elastic strain of the myosin filament, was less steeply dependent on the size of the applied length step.

We used these experimental values of I_{HA}/I_{LA} and S_{M3} to calculate the interference distance L and the myosin head spacing d using the theoretical intensity distributions described above (Fig. 1c). These equations would only apply exactly if each layer of myosin heads could be considered as a point mass, but a similar analysis using the axial mass projections of atomic models for the myosin head[5–7] gave the same values of I_{HA}/I_{LA} and S_{M3} within the precision of the present measurements[18]. The changes in L can therefore be interpreted solely in terms of the average axial motion (Δc) of the centres of mass of the myosin heads with respect to their attachments to the myosin filament, independent of any other effects of changes in their conformation.

The X-ray interference method allows Δc to be measured with a precision of about 1 Å (Fig. 3a). Δc was roughly proportional to the extent of the shortening step for steps of up to 7 nm per half-sarcomere, but was about five times smaller than the imposed filament sliding. The value of Δc at T_2 (Fig. 3a, blue triangles) was similar to that at T_1 (red circles). This result is consistent with models in which force is generated in phase 2 by a working stroke in actin-attached myosin heads, but is not consistent with models that lack a working stroke.

In both types of model Δc is expected to decrease in phase 1, because actin-attached myosin heads are carried towards the centre of the myosin filament during muscle shortening. In working stroke models, the heads remain attached to actin in phase 2; there is no filament sliding in this period and so, neglecting for the moment any effects of filament compliance, the actin-binding sites of the heads would remain at the same distance from the centre of the myosin filament. In contrast, in models without a working stroke force is simply proportional to the strain in the head; thus, force generation in phase 2 would be accompanied by myosin heads binding to new actin sites that were, on average, farther from the centre of the myosin filament. This would produce an increase in Δc during phase 2, which was not observed (Fig. 3a).

To make a quantitative interpretation of the observed axial

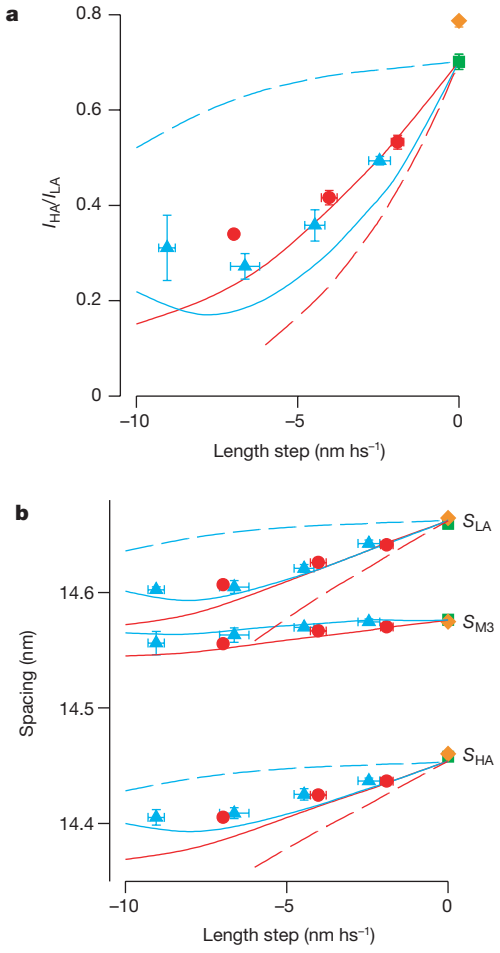

Figure 2 Relative intensity and spacings of the higher (HA) and lower (LA) angle peaks of the M3 reflection. **a**, Relative intensity; **b**, spacings. S_{M3}, weighted mean spacing. Red circles (T_1) and blue triangles (T_2) are the means ± s.e.m. for $n = 3–6$ fibres, except for the T_1 point at −7 nm per half-sarcomere ($n = 1$). Green squares denote values for the 2-ms period before the length step (T_0, Fig. 1a); orange diamonds are values from contractions without imposed length steps. The lines were calculated from the simulations described in the text: red, T_1; blue, T_2. Continuous lines indicate that only one head of each myosin responds to the length step; red dashed line (T_1) indicates that all heads in the fibre respond to the step; blue dashed line (T_2) indicates the rapid detachment/attachment model.

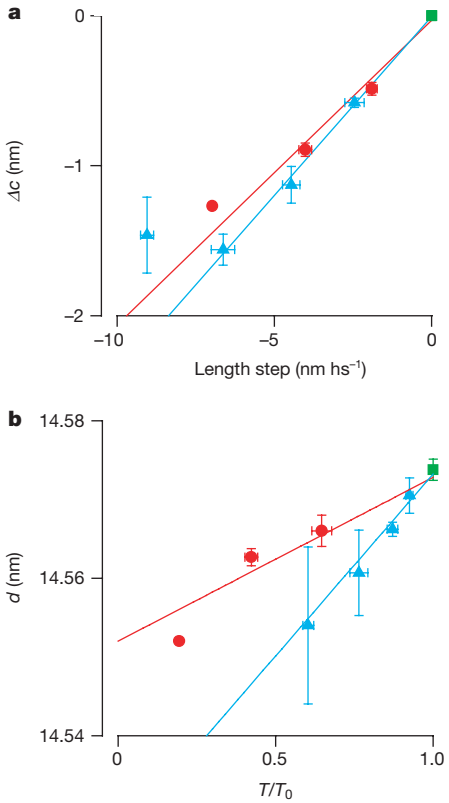

Figure 3 Axial motions and spacings of myosin heads. **a**, Axial motions (Δc) of myosin head centroids with respect to their myosin filament attachments. **b**, Axial spacing of the heads along the myosin filament (d) plotted against normalized force T/T_0. Parameters Δc and d were obtained for each fibre and condition by fitting experimental values of I_{HA}/I_{LA} and S_{M3} (Fig. 2) for each fibre. A negative value of Δc denotes motion towards the centre of the myosin filament. See Fig. 2 for definition of symbols. The lines were obtained by linear regression of all individual fibre data except the T_2 points in the −9 nm per half-sarcomere class in **a**.

motions of the myosin heads (Δc), the compliance of the actin and myosin filaments must be taken into account. The filament compliances are usually expressed as the average strain in the actin or myosin filament, $\langle S_A \rangle$ or $\langle S_M \rangle$, owing to the active isometric force (T_0). $\langle S_A \rangle$ is 0.26%/T_0 in the conditions used here[20,21]. $\langle S_M \rangle$ is the slope of the relationship between the myosin filament periodicity d and the normalized force T/T_0. $\langle S_M \rangle$ was 0.14 ± 0.03%/T_0 at T_1 (Fig. 3b, red circles, $n = 9$ fibres) and 0.34 ± 0.05%/T_0 at T_2 (blue triangles, $n = 18$).

The value of $\langle S_M \rangle$ at T_1 represents the instantaneous compliance of the myosin filament, and the higher value at T_2 is likely to include a contribution from changes in the structure of the myosin filament[18,22]. The total instantaneous compliance of each set of overlapping myosin and actin filaments crosslinked by myosin heads during active isometric contraction is 5.1 nm/T_0. Of this, roughly 40% is due to the compliance of the actin filaments, 20% to that of the myosin filaments, and 40% to that of the myosin heads[20,21].

We calculated the axial displacement of each layer of myosin heads along the filament during the elastic phase 1 response to a length step from these filament and myosin head compliances. These motions occur to the same extent in models with and without a working stroke, so the phase 1 analysis provides an independent calibration of the X-ray interference method. Each layer of heads was represented by an atomic model with the catalytic domain in its nucleotide-free conformation[5,6] and a variable bend between the catalytic and light chain domains[7,8] (see Methods). The changes in I_{HA}/I_{LA}, S_{LA} and S_{HA} calculated from this model (Fig. 2, red dashed lines) were much larger than the observed changes (red circles).

The discrepancy is too large to be explained by uncertainty about the location of the pivot in the myosin head; it was reduced by only about a quarter when the pivot was assumed to be at the actin-binding site. Moreover, the discrepancy cannot be explained by possible errors in the values of filament compliance. The calculated values of I_{HA}/I_{LA}, S_{LA} and S_{HA} are almost independent of the value of $\langle S_M \rangle$, because myosin filament compliance leads to proportional changes in d and L (ref. 18). The discrepancy is reduced by increasing the value of $\langle S_A \rangle$, but would not be eliminated even if $\langle S_A \rangle$ were twice the measured value[20,21], in which case almost the whole compliance of the muscle sarcomere would be in the filaments, with virtually no contribution left for the myosin heads.

We conclude that this type of model, in which the M3 reflection is solely due to the myosin heads, and all the myosin heads in the fibre respond to filament sliding, is incompatible with the observed changes in the fine structure of the M3 reflection. It is unlikely that other structures in the fibre make a substantial contribution to the active M3 reflection, because the reflection can be almost completely abolished by extended high-velocity shortening[22]. Moreover, the linear dependence of the intensity of the active M3 reflection on the degree of overlap between the myosin and actin filaments[18] shows that it originates from the part of the myosin filament that overlaps with actin, and that detached myosin heads in the region of the filament that does not overlap with actin are too disordered to make a significant contribution.

Thus, the smaller-than-expected changes in interference fine structure observed during length steps show that there is a population of myosin heads in the overlap region that do not respond to filament sliding, although they have sufficient axial order to contribute to the M3 reflection. Because each myosin molecule has two heads, these static heads are likely to be the partners of heads that are attached to actin. The two heads are joined at the head–tail junction, so attachment of one head to actin would impose axial order on the other head, and both would contribute to the M3 X-ray reflection. Adding the partner heads to the model gave a reasonably good fit to the observed changes in I_{HA}/I_{LA}, S_{LA} and S_{HA} at T_1 (Fig. 2, red continuous lines), especially considering that there are no adjustable parameters in the model. Thus the elastic, phase 1 changes in the interference fine structure can be explained quantitatively if only one head of each myosin molecule bears the force of isometric contraction and responds to filament sliding.

Finally, we return to the quantitative explanation of the origin of rapid force recovery in phase 2 of the force transient. If, as argued above, only one head of each myosin responds to the length step, would a working stroke in this head reproduce the observed values of I_{HA}/I_{LA}, S_{LA} and S_{HA} at T_2? The calculated values for T_2 for the working stroke model (Fig. 2, blue continuous lines) gave a good but not perfect fit to the experimental data (blue triangles). In contrast, the rapid attachment/detachment model (Fig. 2, blue dashed lines) was clearly inconsistent with the observed changes, independent of the magnitude of filament compliance. The imperfect fit of the working stroke model at T_2 is probably caused by a small fraction of heads detaching during phase 2; both stiffness measurements[11] and changes in the intensity of the M3 reflection produced by closely spaced pairs of length steps[12] suggest that about 8% of the heads have detached by T_2 after a 5-nm shortening step and have become disordered axially, so that they no longer contribute to the M3 reflection or to the axial displacement Δc measured from its interference fine structure.

Most of the heads behave as predicted by the working stroke model. This model reproduces the observed nonlinear dependence of the interference parameters on the size of length step, and the approximate fit was maintained for the largest releases studied (9 nm). Thus, our results provide strong support for working stroke models in which myosin heads remain attached during filament sliding of about 10 nm, and are clearly inconsistent with models in which force is generated by rapid attachment and detachment of myosin and actin. □

Methods

Mechanical measurements

Single fibres from the anterior tibialis muscle of *Rana temporaria* were mounted horizontally between a loudspeaker coil motor and a capacitance gauge force transducer[23] at sarcomere length 2.1 μm, 4 °C, and electrically stimulated for 2.3 s at 18–25 Hz. After 0.3 s of isometric contraction, forty 50-ms shortening/stretch cycles were imposed with a 4-ms interval between shortening and stretch[12]. We measured sarcomere length continuously in a segment of 1–2 mm near the fibre centre with a striation follower[24].

X-ray data collection

The fibre and mechanical apparatus were mounted vertically on X-ray beamline ID2A of the European Synchrotron Radiation Facility (ESRF), Grenoble, France[25]. The X-ray beam had a full width at half maximum (FWHM) of about 0.1 mm vertically and 0.6 mm horizontally, a flux of up to 2×10^{13} photons s^{-1} and a wavelength of 0.1 nm. We controlled X-ray exposure with 10-μs precision by two electromagnetic shutters in series. Diffraction patterns were recorded on A3-size storage PhosphorImage plates (Molecular Dynamics) mounted in an evacuated camera tube 9.85 m from the fibre. Image plates were scanned off-line (Molecular Dynamics 840 scanner) with 100-μm pixels. The vertical point spread function of the X-ray camera/scanner combination had FWHM 320 μm.

Experimental protocol

We stimulated fibres at 4-min intervals and moved them vertically by 100–250 μm between contractions to spread the effects of radiation damage. Diffraction data for 100-μs exposures were typically accumulated from 40 length steps in each of 20 contractions with the unattenuated X-ray beam (total exposure 80 ms). For 2-ms exposures, we used 40 length steps, 4 contractions and 4× beam attenuation. Diffraction data during isometric contraction were recorded with 200-ms exposures, 4 contractions and 7× beam attenuation. Total X-ray exposure per fibre was typically equivalent to 0.5 s of unattenuated beam. Experiments were terminated by failure of excitation–contraction coupling; up to this point X-ray and mechanical responses were stable. Data are presented from 18 fibres with a cross-sectional area of 22,500 ± 5,800 μm^2 (mean ± s.d.)

X-ray data analysis

We analysed X-ray diffraction patterns with the programs HV (A. Stewart, Brandeis), Fit2D (A. Hammersley, ESRF) and Peakfit (SPSS Science). Patterns were aligned and centred using the 1,0 equatorial reflections. The background under the axial X-ray

reflections was subtracted using HV. The axial intensity distribution was calculated by radial integration from ± 1/64 nm^{-1} and the M3 reflection fitted by two gaussian peaks using Peakfit. We calculated the M3 spacing (S_{M3}) as the intensity-weighted mean of that of the two peaks. Spacings were calibrated assuming that S_{M3} is 14.340 nm at rest[26] or 14.573 nm during active isometric contraction[18].

Simulation of the axial intensity distribution

The interference fine structure of the M3 reflection was calculated as the Fourier transform of the axial mass distribution. Each myosin filament was assumed to contain two arrays of myosin heads separated by a bare zone[27,28] of length B (~160 nm). Each array has 49 layers of heads with axial periodicity d. The axial mass projection of each layer of heads was calculated from crystallographic data, with the catalytic domain (CD, heavy chain residues 1–707) of the head in its nucleotide-free actin-bound conformation[5,6], and the light chain domain (LCD, heavy chain residues 707–843 and both light chains) tilted axially around the CD/LCD junction[7,8,12]. During isometric contraction the 707–843 axis was assumed to be at 60° to the filament axis[12]. LCD tilt dispersion of ± 20°, which would allow myosin heads to bind to actin monomers with axial periodicity of 5.5 nm, had a negligible effect on the results[12].

We used a distributed filament compliance formalism[21,29,30] to calculate the force and strain distribution along the myosin and actin filaments. The strain in myosin heads during isometric contraction was assumed to be uniform along the filament overlap zone. Rapid force recovery after a length step was assumed to be due to a uniform force contribution from heads along the overlap zone. We calculated the mass distribution along the filament with the position of the head–rod junction of each level of heads determined by the myosin filament strain; head strain was represented as a tilt of the LCD with respect to the actin-bound CD[5]. In the working stroke model, the distribution of myosin head strain along the overlap zone after a length step was calculated under the constraint of constant sarcomere length during rapid force recovery. Force recovery during the 110-μs length step itself was estimated from the difference between the measured force (T_1) and that expected from the instantaneous half-sarcomere compliance (5.1 nm/T_0; ref. 20) and taken into account in calculating the mass distribution at T_1. Simulations using the rapid detachment/attachment model assumed that the total fraction of myosin heads attached to actin remained constant and that the average head strain was proportional to the force.

Received 24 July; accepted 3 December 2001.

1. Huxley, A. F. Muscle structure and theories of contraction. *Prog. Biophys. Biophys. Chem.* **7,** 255–318 (1957).
2. Huxley, H. E. The mechanism of muscle contraction. *Science* **164,** 1356–1366 (1969).
3. Huxley, A. F. & Simmons, R. M. Proposed mechanism of force generation in striated muscle. *Nature* **233,** 533–538 (1971).
4. Huxley, A. F. Muscular contraction (review lecture). *J. Physiol. (Lond.)* **243,** 1–43 (1974).
5. Rayment, I. *et al.* Three-dimensional structure of myosin subfragment-1: a molecular motor. *Science* **261,** 50–58 (1993).
6. Rayment, I. *et al.* Structure of the actin–myosin complex and its implications for muscle contraction. *Science* **261,** 58–65 (1993).
7. Dominguez, R., Freyzon, Y., Trybus, K. M. & Cohen, C. Crystal structure of a vertebrate smooth muscle myosin motor domain and its complex with the essential light chain: visualisation of the pre-power stroke state. *Cell* **94,** 559–571 (1998).
8. Geeves, M. A. & Holmes, K. C. Structural mechanism of muscle contraction. *Annu. Rev. Biochem.* **68,** 687–728 (1999).
9. Huxley, H. E. *et al.* Changes in the X-ray reflections from contracting muscle during rapid mechanical transients and their structural implications. *J. Mol. Biol.* **169,** 469–506 (1983).
10. Irving, M., Lombardi, V., Piazzesi, G. & Ferenczi, M. A. Myosin head movements are synchronous with the elementary force-generating process in muscle. *Nature* **357,** 156–158 (1992).
11. Lombardi, V., Piazzesi, G. & Linari, M. Rapid regeneration of the actin–myosin power stroke in contracting muscle. *Nature* **355,** 638–641 (1992).
12. Irving, M. *et al.* Conformation of the myosin motor during force generation in skeletal muscle. *Nature Struct. Biol.* **7,** 482–485 (2000).
13. Corrie, J. E. T. *et al.* Dynamic measurement of myosin light-chain domain tilt and twist in muscle contraction. *Nature* **400,** 425–430 (1999).
14. Podolsky, R. J. & Nolan, A. C. Muscle contraction transients, cross-bridge kinetics, and the Fenn effect. *Cold Spring Harb. Symp. Quant. Biol.* **37,** 661–668 (1973).
15. Brenner, B. Rapid dissociation and reassociation of actomyosin cross-bridges during force generation: a newly observed facet of cross-bridge action in muscle. *Proc. Natl Acad. Sci. USA* **88,** 10490–10494 (1991).
16. Kitamura, K., Tokunaga, M., Iwane, A. H. & Yanagida, T. A single myosin head moves along an actin filament with regular steps of 5.3 nanometres. *Nature* **397,** 129–134 (1999).
17. Howard, J. *Mechanics of Motor Proteins and the Cytoskeleton* (Sinauer, Sunderland, MA, 2001).
18. Linari, M. *et al.* Interference fine structure and sarcomere length dependence of the axial X-ray pattern from active single muscle fibres. *Proc. Natl Acad. Sci. USA* **97,** 7226–7231 (2000).
19. Ford, L. E., Huxley, A. F. & Simmons, R. M. Tension responses to sudden length change in stimulated frog muscle fibres near slack length. *J. Physiol. (Lond.)* **269,** 441–515 (1977).
20. Dobbie, I. *et al.* Elastic bending and active tilting of myosin heads during muscle contraction. *Nature* **396,** 383–387 (1998).
21. Linari, M. *et al.* The stiffness of skeletal muscle in isometric contraction and rigor: the fraction of myosin heads bound to actin. *Biophys. J.* **74,** 2459–2473 (1998).
22. Piazzesi, G. *et al.* Changes in conformation of myosin heads during the development of isometric contraction and rapid shortening in single frog muscle fibres. *J. Physiol. (Lond.)* **514,** 305–312 (1999).
23. Lombardi, V. & Piazzesi, G. The contractile response during steady lengthening of stimulated frog muscle fibres. *J. Physiol. (Lond.)* **431,** 141–171 (1990).
24. Huxley, A. F., Lombardi, V. & Peachey, L. D. A system for fast recording of longitudinal displacement of a striated muscle fibre. *J. Physiol. (Lond.)* **317,** 12P–13P (1981).
25. Boesecke, P., Diat, O. & Rasmussen, B. High-brilliance beamline at the European Synchrotron Radiation Facility. *Rev. Sci. Instrum.* **66,** 1636–1638 (1995).
26. Haselgrove, J. C. X-ray evidence for conformational changes in the myosin filaments of vertebrate striated muscle. *J. Mol. Biol.* **92,** 113–143 (1975).
27. Sjöström M. & Squire, J. M. Fine structure of the A band in cryosections: the structure of the A-band of human skeletal muscle fibres from ultrathin cryosections negatively stained. *J. Mol. Biol.* **109,** 49–68 (1977).
28. Craig, R. Structure of A-segments from frog and rabbit skeletal muscle. *J. Mol. Biol.* **109,** 69–81 (1977).
29. Thorson, J. W. & White, D. C. S. Distributed representations for actin-myosin interaction in the oscillatory contraction of muscle. *Biophys. J.* **9,** 360–390 (1969).
30. Ford, L. E., Huxley, A. F. & Simmons, R. M. The relation between stiffness and filament overlap in stimulated frog muscle fibres. *J. Physiol. (Lond)* **311,** 219–249 (1981).

Acknowledgements

This work was supported by the Medical Research Council, Consiglio Nazionale delle Ricerche (CNR), Ministero dell'Istruzione, dell'Università e della Ricerca (MURST), Telethon (Italy), EMBL, EU and ESRF. We thank A. F. Huxley for comments, J. Gorini, A. Aiazzi and M. Dolfi for mechanical and electronics support.

Competing interests statement

The authors declare that they have no competing financial interests.

Correspondence and requests for materials should be addressed to M.I. (e-mail: malcolm.irving@kcl.ac.uk).

RanGAP mediates GTP hydrolysis without an arginine finger

Michael J. Seewald, Carolin Körner, Alfred Wittinghofer & Ingrid R. Vetter

Max-Planck-Institut für molekulare Physiologie, Abteilung Strukturelle Biologie, Postfach 102664, D-44026 Dortmund, Germany

GTPase-activating proteins (GAPs) increase the rate of GTP hydrolysis on guanine nucleotide-binding proteins by many orders of magnitude. Studies with Ras and Rho have elucidated the mechanism of GAP action by showing that their catalytic machinery is both stabilized by GAP binding and complemented by the insertion of a so-called 'arginine finger' into the phosphate-binding pocket[1,2]. This has been proposed as a universal mechanism for GAP-mediated GTP hydrolysis. Ran is a nuclear Ras-related protein that regulates both transport between the nucleus and cytoplasm during interphase, and formation of the mitotic spindle and/or nuclear envelope in dividing cells[3]. Ran–GTP is hydrolysed by the combined action of Ran-binding proteins (RanBPs) and RanGAP[4]. Here we present the three-dimensional structure of a Ran–RanBP1–RanGAP ternary complex in the ground state and in a transition-state mimic. The structure and biochemical experiments show that RanGAP does not act through an arginine finger, that the basic machinery for fast GTP hydrolysis is provided exclusively by Ran and that correct positioning of the catalytic glutamine is essential for catalysis.

Ran-mediated GTP hydrolysis is thought to be the main driving force behind cargo transport across the nuclear pore complex. The location of the Ran-specific guanine nucleotide exchange factor RCC1 in the nucleus and that of RanGAP in the cytoplasm creates a gradient of Ran–GTP across the nuclear pore complex. The GTP-bound form of Ran in the nucleus binds with high affinity to the import receptors of the importin-β family and thereby induces the release of import cargo, whereas export cargo binding to export receptors (exportins) requires the presence of Ran–GTP[3]. The